International Journal for Multiscale Computational Engineering, 5(1)1–10(2007)

Numerical Methods for Reacting Gas Flow Simulations

S. van Veldhuizen & C. Vuik*

Department of Applied Mathematics and J.M. Burgers Center for Fluid Mechanics, Delft University of Technology, Mekelweg 4, 2628 CD Delft, The Netherlands

C. R. Kleijn

Department of Multiscale Physics and J.M. Burgers Center for Fluid Mechanics, Delft University of Technology, Prins Bernardlaan 6, 2628 BW Delft, The Netherlands

ABSTRACT

In this study, various numerical schemes for transient simulations of 2D laminar reacting gas flows, as typically found in chemical vapor deposition reactors, are proposed and compared. These systems are generally modeled by means of many stiffly coupled elementary gas phase reactions between a large number of reactants and intermediate species. The purpose of this study is to develop robust and efficient solvers for the stiff reaction system, where as a first approach the velocity and temperature fields are assumed to be given. In this paper, we mainly focus on the performance of different time integration methods and their properties to successfully solve the transient problem. Besides stability, which is important due to the stiffness of the problem, the preservation of nonnegativity of the species is crucial. It appears that this latter condition on time integration methods is much more restrictive toward the time step than stability.

*Address all correspondence to s.vanveldhuizen@tudelft.nl

1543-1649/06/$35.00

1. INTRODUCTION

Chemical vapor deposition (CVD) is a process that uses chemically reacting gases to deposit thin solid films on a solid material. A CVD system consists of a chemical reactor in which precursor gases containing the atoms to be deposited are introduced, usually diluted in an inert carrier gas. The deposition on a solid surface is due to chemical reactions, which are usually driven by thermal energy. Applications of thin solid films can be found in various technological areas such as microelectronics (semiconductors), optical devices (mirror and/or lens coatings), and as decorative or protective coatings in, for instance, the ceramics and glass industries [1].

In the literature on simulation of CVD, and also other reactive flows, one is usually looking for the steady-state solution of the species equations. The usual procedure to find this steady-state solution is to perform a (damped/relaxed) Newton iteration with an (arbitrary) initial solution. Hopefully, the Newton iteration converges to the steady-state. If this is not the case, one performs some (artificial) time stepping in order to find a better initial solution for the next Newton iteration [2,3].

CVD is a typical example of a multiscale problem, i.e., the time scales of advection and diffusion often differ in orders of magnitude from the time scales of the chemical reactions. The resulting system of advection-diffusion-reaction equations that describe the transport of the chemical species, due to advection and diffusion, and their conversion due to the chemical reactions is extremely stiff. For typical CVD simulations where the number of species is in the range 25–100, and the number of grid points in each spatial direction between 30 and 100, simulations are usually limited to 2D and mostly steady-state. It is our aim to perform multidimensional transient CVD simulations. Therefore, a suitable time integration method has to be selected to stably integrate the stiff system of species equations. The time integration method should also conserve the nonnegativity of the species. This so-called positivity property appears to be more restrictive towards the time step size than stability. Of course, other important criteria for transient solvers are efficiency and robustness.

2. MODEL FOR CVD SIMULATION

The mathematical model describing a CVD process consists of a set of PDEs with appropriate boundary and initial conditions, which describe the gas flow, the transport of energy, the transport of species, and reactions in the reactor. The gas mixture in the reactor is assumed to behave as a continuum. The gas flow in the reactor is assumed to be incompressible and laminar. Viscous heating due to dissipation and the effects of pressure variations in the energy equation can be neglected for low viscosity, low Mach number flows. The composition of the N-component gas mixture is described in terms of the dimensionless mass fractions $\omega_i = \rho_i/\rho$, $i = 1, \ldots, N$, having the property $\sum_{i=1}^{N} \omega_i = 1$. The transport of mass, momentum, and heat are described, respectively, by the continuity equation, the Navier-Stokes equations, and the transport equation for thermal energy expressed in terms of temperature T. See, for instance, [3].

We assume that in the gas-phase K reversible reactions of the form

$$\sum_{i=1}^{N} \nu'_{ik} A_i \underset{k^g_{k,\text{backward}}}{\overset{k^g_{k,\text{forward}}}{\rightleftarrows}} \sum_{i=1}^{N} \nu''_{ik} A_i \tag{1}$$

take place. In (1), $\mathcal{A}_i$ are the species in the gas mixture, ν'_{ik} the forward stoichiometric coefficient for species i in reaction k, and ν''_{ik} the backward stoichiometric coefficient for species i in the kth reaction. The net stoichiometric coefficient is defined as $\nu_{ik} = \nu''_{ik} - \nu'_{ik}$. For the kth reaction the *net* molar reaction rate R^g_k $\left(\text{mole}/\text{m}^3 \cdot \text{s}\right)$ is defined as

$$R^g_k = k^g_{k,\text{forward}} \prod_{i=1}^{N} \left(\frac{P \omega_i m}{RT m_i} \right)^{\nu'_{ik}} - k^g_{k,\text{backward}} \prod_{i=1}^{N} \left(\frac{P \omega_i m}{RT m_i} \right)^{\nu''_{ik}} \tag{2}$$

where the forward reaction rate constant $k^g_{k,\text{forward}}$ is fitted according to a modified Arrhenius expression

$$k^g_{k,\text{forward}}(T) = A_k T^{\beta_k} e^{-E_k/RT} \tag{3}$$

The backward reaction rate constant $k^g_{k,\text{backward}}$ are computed self-consistently from thermochemistry, according to

$$k^g_{\text{backward}}(T) = \frac{k^g_{\text{forward}}(T)}{K^g(T)} \left(\frac{RT}{P^0}\right)^{\sum_{i=1}^{N} \nu_{ik}} \tag{4}$$

with $K^g(T)$ the reaction equilibrium constants.

The mass diffusion flux is decomposed into concentration diffusion and thermal diffusion. In this study, we describe ordinary diffusion in terms of effective diffusion coefficients $\mathbb{D}'_i$, such that we obtain for species transport in the reactor

$$\frac{\partial(\rho\omega_i)}{\partial t} = -\nabla\cdot(\rho\mathbf{v}\omega_i) + \nabla\cdot(\rho\mathbb{D}'_i\nabla\omega_i) + \nabla\cdot\left[\mathbb{D}^T_i\nabla(\ln T)\right] + m_i\sum_{k=1}^{K}\nu_{ik}R^g_k \tag{5}$$

where $\mathbb{D}^T_i$ is the multicomponent thermal diffusion coefficient for species i.

The main focus of our research is on efficient solvers for the above species equations (5). A detailed description of the physics involved and the boundary conditions can be found in [4].

3. REACTOR CONFIGURATION AND CHEMISTRY MODEL

In addition to the transport model as has been described in the previous section, we provide details on the reactor configuration and the chemistry model involved. Both the reactor configuration and the chemistry model are taken from [3]. For a simpler test problem, we refer to [5,6].

3.1 Reactor Configuration

The reactor geometry is presented in Fig. 1. The computational domain is, because of axisymmetry, one half of the $(r\text{-}z)$ plane. The pressure in the reactor is 1 atm. From the top, a gas mixture, consisting of 0.1 mole$\%$ diluted in helium enters the reactor with a uniform temperature $T_{\text{in}} = 300$ K and velocity $u_{\text{in}} = -0.1\text{m/s}$. At a distance of 10 cm below the inlet, a (nonrotating) susceptor with temperature $T_s = 1000$ K and a diameter of 30 cm is placed.

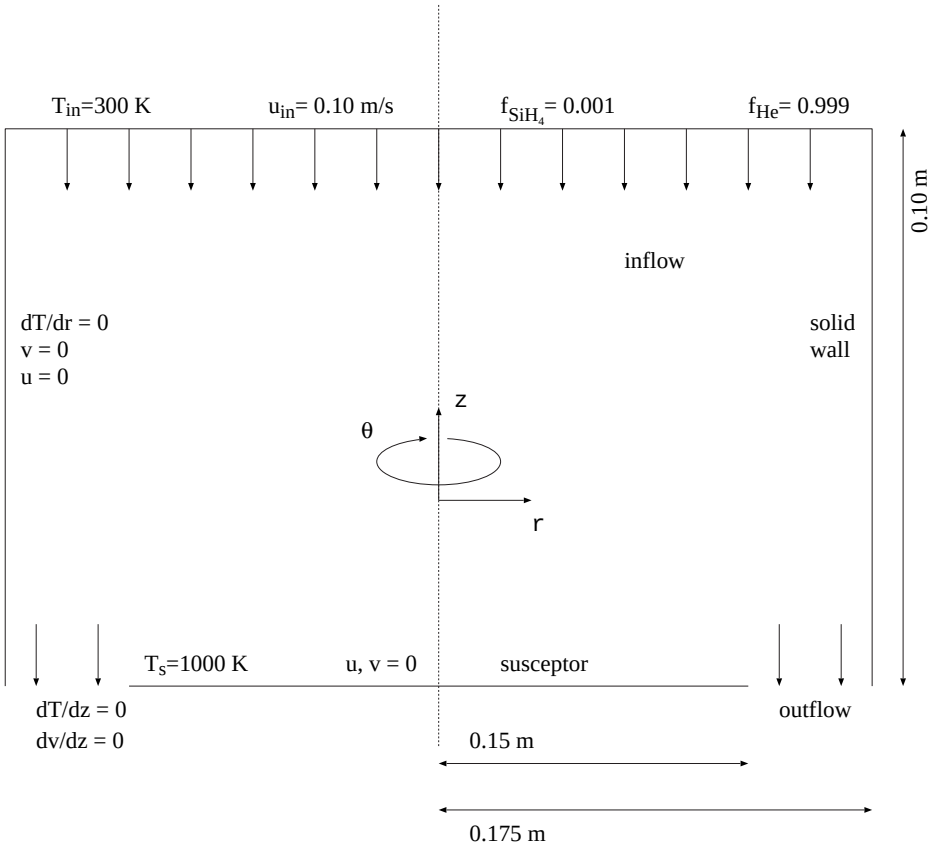

FIGURE 1. Reactor geometry

3.2 Chemistry Model

In the hot gas region above the susceptor, the reactive species silane SiH_4 decomposes into silylene SiH_2 and hydrogen gas H_2. This gas phase reaction initiates a chain of 25 homogeneous gas phase reactions leading to the (de)formation of silicon-containing gas species. Each of these species may diffuse to the susceptor to form solid silicon.

3.2.1 Gas Phase Chemistry

The 26 gas phase reactions between the 17 gas phase species in this chemistry model, taken from [3,7], are listed in Table 1. The reaction terms in Eq. (5) are constructed as in Eqs. (2)–(4), where the fit parameters can be found in Table 1. The backward reaction rates are computed via Eq. (4), where the reaction equilibrium K^g is approximated as

$$K^g(T) = A_{\mathrm{eq}} T^{\beta_{\mathrm{eq}}} e^{-E_{\mathrm{eq}}/RT} \tag{6}$$

The fit parameters of Eq. (6) can be found in Table 1.

3.2.2 Surface Chemistry

Because of the modeled chain of gas phase reactions initiated by the decomposition of silane, the gas mixture in the reactor contains 14 different silicon-containing species, which each may diffuse toward the wafer surface to produce a thin film of solid silicon. Film growth is due to irreversible, unimolecular decomposition reactions of silicon-containing species at the surface, due to one of the following surface reactions:

$$\mathrm{Si}_n\mathrm{H}_{2m} \overset{R^S_{\mathrm{Si}_n\mathrm{H}_{2m}}}{\longrightarrow} n\ \mathrm{Si\ (s)} + m\ \mathrm{H_2\ (g)} \tag{7}$$

$$\mathrm{Si}_n\mathrm{H}_{2m+1} \overset{R^S_{\mathrm{Si}_n\mathrm{H}_{2m+1}}}{\longrightarrow} n\ \mathrm{Si\ (s)} + m\ \mathrm{H_2\ (g)} + \mathrm{H\ (g)} \tag{8}$$

with $n = 1, 2, 3$ and $m = 0, 1, 2, 3, 4$. In surface reactions (7) and (8), we have besides the deposition of silicon also desorption of gaseous hydrogen. The stoichiometric coefficients will follow immediately from reactions (7) and (8). The molar reaction rate R_i^S for the decomposition of gas species i is given as

$$R_i^S = \frac{\gamma_i}{1 - (\gamma_i/2)} \frac{P f_i}{(2\pi m_i R T_s)^{1/2}} \tag{9}$$

where γ_i is the sticking coefficient of species i, and T_s the temperature of the wafer surface [3]. The sticking coefficients are for all silicon-containing species equal to one, except for $\gamma_{\mathrm{Si_3H_8}} = 0$, $\gamma_{\mathrm{Si_2H_6}} = 0.537\exp^{-9400/T_s}$ and $\gamma_{\mathrm{SiH_4}} = (1/10)\gamma_{\mathrm{Si_2H_6}}$. The growth rate $\mathcal{G}_{\mathrm{Si}}$ of solid silicon Si is defined as

$$\mathcal{G}_{\mathrm{Si}} = \frac{m_{\mathrm{Si}}}{\rho_{\mathrm{Si}}} \sum_{s=1}^{S} R_s^S \chi_n \tag{10}$$

with n the number of silicon atoms in the reacting species, according to Eqs. (7) and (8). More background information can be found in, for example, [2–4]. The finite volume discretization of the boundary condition for the reacting surface can be found in [8].

4. CONSERVATION OF THE POSITIVITY OF THE SPECIES CONCENTRATIONS

To numerically solve the species equations, we apply the method of lines, i.e., we first discretize in space, to yield a semidiscrete system

$$w'(t) = F[t, w(t)], \quad 0 < t \le T \tag{11}$$

where $w(0)$ is given.

Details on the spatial discretization can be found in [4]. The MOL approach is further discussed in [8]. The next step is to apply a suitable ODE method to integrate Eq. (11).

Following [9], we say that stiffness indicates a class of problems for which implicit methods perform (much) better than explicit methods. The eigenvalues of the Jacobian $\delta f/\delta y$ certainly play a role in this decision, but quantities such as the dimension of the system and the smoothness of the solution are also important. Therefore, the stiff reaction terms in CVD chemistry models motivates to integrate (parts of) $F[t, w(t)]$ implicitly. Besides the stability issue, we also want to conserve the physical interpretation of the species concentrations. This means that we demand preservation of their nonnegativity during transient simulation. In this section we discuss this property mainly for time integration and discover it is not easily satisfied for stiff chemistry problems.

4.1 Positive Time Stepping

The natural nonnegativity of the mass fractions should be preserved within the mathematical

TABLE 1. Fit parameters for the forward reaction rates (4) and gas phase equilibria constants (6) for the benchmark problem. The parameters A_k, β_k, A_{eq}, and β_{eq} are dimensionless, while E_k and E_{eq} have units of $\mathrm{kJ/mol}$. Note that the corresponding table in [3] contains a number of typographical and printing errors, which have been corrected the present table

Reaction	A_k	β_k	E_k	$A_{k,eq}$	$\beta_{k,eq}$	$E_{k,eq}$
$SiH_4 \rightleftharpoons SiH_2 + H_2$	1.09×10^{25}	-3.37	256	6.85×10^{5}	0.48	235
$SiH_4 \rightleftharpoons SiH_3 + H$	3.69×10^{15}	0.0	390	1.45×10^{4}	0.90	382
$Si_2H_6 \rightleftharpoons SiH_4 + SiH_2$	3.24×10^{29}	-4.24	243	1.96×10^{12}	-1.68	229
$SiH_4 + H \rightleftharpoons SiH_3 + H_2$	1.46×10^{7}	0.0	10	1.75×10^{3}	-0.55	-50
$SiH_4 + SiH_3 \rightleftharpoons Si_2H_5 + H_2$	1.77×10^{6}	0.0	18	1.12×10^{-6}	2.09	-6
$SiH_4 + SiH \rightleftharpoons Si_2H_3 + H_2$	1.45×10^{6}	0.0	8	1.82×10^{-4}	1.65	21
$SiH_4 + SiH \rightleftharpoons Si_2H_5$	1.43×10^{7}	0.0	8	1.49×10^{-10}	1.56	-190
$SiH_2 \rightleftharpoons Si + H_2$	1.06×10^{14}	-0.88	189	1.23×10^{2}	0.97	180
$SiH_2 + H \rightleftharpoons SiH + H_2$	1.39×10^{7}	0.0	8	2.05×10^{1}	-0.51	-101
$SiH_2 + H \rightleftharpoons SiH_3$	3.81×10^{7}	0.0	8	2.56×10^{-3}	-1.03	-285
$SiH_2 + SiH_3 \rightleftharpoons Si_2H_5$	6.58×10^{6}	0.0	8	1.75×10^{-12}	1.60	-241
$SiH_2 + Si_2 \rightleftharpoons Si_3 + H_2$	3.55×10^{5}	0.0	8	5.95×10^{-6}	1.15	-225
$SiH_2 + Si_3 \rightleftharpoons Si_2H_2 + Si_2$	1.43×10^{5}	0.0	68	2.67×10^{0}	-0.18	59
$H_2SiSiH_2 \rightleftharpoons Si_2H_2 + H_2$	3.16×10^{14}	0.0	222	1.67×10^{6}	-0.37	112
$Si_2H_6 \rightleftharpoons H_3SiSiH + H_2$	7.94×10^{15}	0.0	236	1.17×10^{9}	-0.36	235
$H_2 + SiH \rightleftharpoons SiH_3$	3.45×10^{7}	0.0	8	1.42×10^{-4}	-0.52	-183
$H_2 + Si_2 \rightleftharpoons Si_2H_2$	1.54×10^{7}	0.0	8	7.47×10^{-6}	-0.37	-216
$H_2 + Si_2 \rightleftharpoons SiH + SiH$	1.54×10^{7}	0.0	168	1.65×10^{3}	-0.91	180
$H_2 + Si_3 \rightleftharpoons Si + Si_2H_2$	9.79×10^{6}	0.0	198	1.55×10^{2}	-0.55	189
$Si_2H_5 \rightleftharpoons Si_2H_3 + H_2$	3.16×10^{14}	0.0	222	1.14×10^{6}	0.08	210
$Si_2H_2 + H \rightleftharpoons Si_2H_3$	8.63×10^{8}	0.0	8	3.43×10^{-4}	-0.31	-149
$H + Si_2 \rightleftharpoons SiH + Si$	5.15×10^{7}	0.0	22	1.19×10^{3}	-0.88	29
$SiH_4 + H_3SiSiH \rightleftharpoons Si_3H_8$	6.02×10^{7}	0.0	0	7.97×10^{-16}	2.48	-233
$SiH_2 + Si_2H_6 \rightleftharpoons Si_3H_8$	1.81×10^{8}	0.0	0	1.36×10^{-12}	1.64	-233
$SiH_3 + Si_2H_5 \rightleftharpoons Si_3H_8$	3.31×10^{7}	0.0	0	1.06×10^{-14}	1.85	-318
$H_3SiSiH \rightleftharpoons H_2SiSiH_2$	1.15×10^{20}	-3.06	28	9.58×10^{-3}	0.50	-50

model, spatial discretization, and time integration of the system. While the first one is obvious, the latter two should not introduce any (small) negative components causing blowup of the solution. It appears that this extra condition on time integration methods is much more restrictive toward the time step than stability.

In order to preserve positivity on the level of spatial discretization we used a hybrid finite volume scheme [4], where the unknown species mass fractions, densities, and temperatures are arranged in a colocated way, and the velocities are staggered. This hybrid scheme approximates the mass fluxes through the cell faces by central differences, and when the cell Peclet number is larger than 2, first-order upwinding is applied. It can be found in [5] that this FV discretization is positive for all spatial meshes.

An ODE system $w'(t) = F[t, w(t)]$, $t \geq 0$, is called positive if $w(0) \geq 0$ implies $w(t) \geq 0$ for all $t > 0$. It is easy to prove that linear systems $w'(t) = Aw(t)$ are positive if and only if $a_{ij} \geq 0$ for $i \neq j$ [5]. For general nonlinear semidiscretizations $w'(t) = F[t, w(t)]$, it appears that unconditional positivity is a very restrictive requirement.

Under the assumption that the nonlinear system arising from the Euler backward (EB) time discretization has a unique solution, it has been proven [9] that EB is positive for every time step size τ. The question a rises whether higher-order time integration schemes exist that are also unconditionally positive. The nonexistence of such a scheme is

shown in [10], where it has been proven that any unconditionally positive time integration method is of order $p \leq 1$. This result implies that EB is the only known time integration scheme being unconditionally positive and that for any higher-order (implicit) time integration method a (tight) condition on the time step size is needed to ensure preservation of nonnegativity, see also Section 5. In [5], the nonexistence of unconditionally positive higher-order (Runge Kutta and/or multistep) time integration methods has been discussed in further detail.

4.2 Positivity for Nonlinear Solvers

The theory on positivity, as presented in the previous section, is not always valid when solving practical problems. For example, the unconditional positivity of EB does not hold in practice. The nonlinear systems arising from the EB time discretization cannot be solved exactly, and therefore one usually applies Newton's method to solve them. The approximated nonlinear solution is not guaranteed to be positive.

In the case that there are negative species concentrations after the nonlinear solver, which are the result of iterative errors within the nonlinear solver, it is justified to set them equal to zero. For instance, negative concentrations as a consequence of rounding errors from the linear solver in the Newton iteration can be set to zero.

In the case of negative entries that cannot be assigned to be rounding errors, our strategy is to redo the time step with halved time step size to enforce positivity. In our experience, this strategy in combination with a variable time step controller, see Section 5, avoids negative concentrations for EB. The strategy as described here, and in more detail in [5], gives a positive solution without clipping, i.e., clipping sets negative concentrations equal to zero and has the disadvantage of adding mass to the system.

4.3 Positivity with Surface Chemistry

Since the species concentrations are computed in the cell centers of the control volumes, the computation of the mass flux due to surface chemistry is not straightforward, in particular, when it needs to preserve positivity. The approach that we used to discretize the reacting wall is taken from [11].

According to Eq. (9), for the type of surface reactions assumed in the present paper, the molar reactive surface flux is linearly proportional to the species molar concentration at the wafer. Consequently, the reactive surface mass flux is linearly proportional to the species mass fraction, and is denoted as $F_{\text{wall}} = K\omega_{\text{wall}}$, with ω_{wall} the unknown species mass fraction at the wafer. Transport phenomena near the wafer consist of diffusion only, since advection is negligible near the wafer [3,4,8]. At the reacting boundary it will hold that the transport mass flux, in this case only due to diffusion, should be equal to F_{wall}, or in discretized form

$$F_{\text{wall}} = \frac{\mathbb{D}}{\Delta z}(\omega_{\text{center}} - \omega_{\text{wall}}) \tag{12}$$

where $\mathbb{D}$ is the total diffusion coefficient, ω_{center} the species mass fraction in the cell center, and Δz the distance from the cell center to the wafer [3,4]. From (12), ω_{wall} can be derived as

$$\omega_{\text{wall}} = \frac{\omega_P}{1 + \frac{\Delta z K}{\mathbb{D}}} \tag{13}$$

It follows from (13) that ω_{wall} is positive when ω_P is positive, and $\omega_{\text{wall}} \leq 1$ as long as $\omega_{\text{center}} \leq 1$. Thus, by replacing the diffusive mass flux by $F_{\text{wall}} = R^S\omega_{\text{wall}}$ with ω_{wall} as in (13), one obtains a positive semidiscretization near the reacting wall. Note that this discretization differs from the one in [4]. Details can be found in [8].

5. SUITABLE TIME INTEGRATION METHODS (TIM)

The topic of this research is to find the most efficient combination of time integration, nonlinear, and linear solvers. Note that if the computational cost of one time step is expensive, then a time integration method that needs more, but computationally cheaper, time steps can be more efficient.

In this section, we briefly present integration methods that are suitable, from a theoretical point of view, for the time integration of the species equations. More comprehensive descriptions can be found in [9]. This section is concluded with the presentation of the nonlinear and linear solvers, and the variable time step size controller as implemented in our code.

5.1 Time Integration Methods

While being unconditionally positive, the EB method has the disadvantage of first-order consistency. In this section, we discuss a selection of higher-order methods, which have good properties in both stability and positivity.

5.1.1 Rosenbrock Methods

The stiff ODE scheme called two-stage Rosenbrock (ROS2), is given by

$$w_{n+1} = w_n + b_1 k_1 + b_2 k_2 \tag{14}$$

$$k_1 = \tau F(w_n) + \gamma\tau \mathbf{A} k_1 \tag{15}$$

$$k_2 = \tau F(w_n + \alpha_{21} k_1) + \gamma_{21}\tau \mathbf{A} k_1 + \gamma\tau \mathbf{A} k_2 \tag{16}$$

where $\mathbf{A} = F'(w_n)$ is the Jacobian matrix of F, and $b_1 = 1 - b_2$, $\alpha_{21} = 1/2b_2$, and $\gamma_{21} = -\gamma/b_2$. The method is second-order consistent for arbitrary γ as long as $b_2 \neq 0$. For $\gamma \geq 1/4$, the method is unconditionally stable and for $\gamma_+ = 1 + (1/2)\sqrt{2}$, the scheme is unconditionally positive for diffusion reaction problems. For advection diffusion reaction problems the ROS2 scheme also performs, quite well, as has been experienced in [12].

5.1.2 Backward Differentiation Formulas (BDF)

The k-step BDF methods are implicit, of order k, and defined as

$$\sum_{j=0}^{k} \alpha_j w_{n+j} = \tau F(t_{n+k}, w_{n+k}), \quad n = 0, 1, \ldots \tag{17}$$

which uses the k past values $w_n, \ldots, w_{n+k-1}$ to compute w_{n+k}. Note that the most advanced level is t_{n+k} instead of t_{n+1}. The 1-step BDF method is backward Euler and the two-step method is

$$\tfrac{3}{2} w_{n+2} - 2 w_{n+1} + \tfrac{1}{2} w_n = \tau F(t_{n+2}, w_{n+2}) \tag{18}$$

Note that the first $(k-1)$ approximations cannot be computed with the k-step BDF scheme, but have to be obtained by another scheme. The time step constraint to be positive for the BDF-2 scheme is twice as strict as for (explicit) Euler Forward scheme. See [5,6,9].

5.1.3 IMEX Runge-Kutta-Chebyshev (IRKC) Methods

The second-order explicit Runge-Kutta-Chebyshev method is given as

$$\begin{aligned}
w_{n0} &= w_n \\
w_{n1} &= w_n + \tilde{\mu}_1 \tau F(t_n + c_0\tau, w_{n0}) \\
w_{nj} &= (1 - \mu_j - \nu_j) w_n + \mu_j w_{n,j-1} + \nu_j w_{n,j-2} \\
&\quad + \tilde{\mu}_1 \tau F(t_n + c_{j-1}\tau, w_{n,j-1}) + \tilde{\gamma}_j \tau F(t_n + c_0\tau, w_{n0}) \\
&\quad j = 1, \ldots, s \\
w_{n+1} &= w_{ns}
\end{aligned} \tag{19}$$

The coefficients $\omega_0, \omega_1, b_j, c_j, \tilde{\mu}_j, \ldots$ can be found in [9]. In Fig. 2, the stability region for $s = 5$ is given. The parameter $\beta(s)$ moves to $-\infty$ when the number of stages s increases, and therefore this scheme is suitable for explicit integration of moderately stiff diffusion terms.

The IMEX extension of the above scheme is as follows. Suppose we have an ODE system $w'(t) = F[t, w(t)]$, with $F[t, w(t)] = F_E[t, w(t)] + F_I[t, w(t)]$. The part $F_I[t, w(t)]$ of $F[t, w(t)]$ is too stiff to be integrated explicitly by the RKC scheme (19) and $F_E[t, w(t)]$ is the moderately stiff part of $F[t, w(t)]$

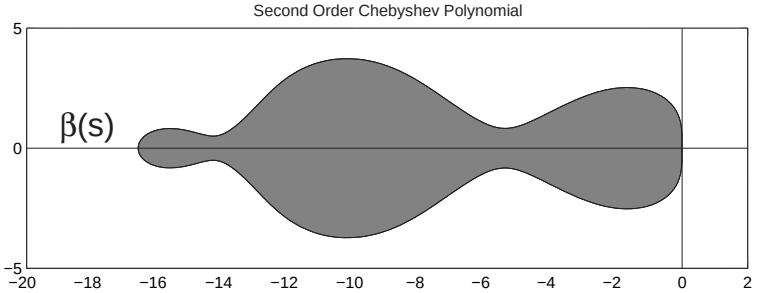

FIGURE 2. Stability region of Eq. (19) with $s = 5$

that can be integrated explicitly by the RKC scheme (19). The first stage of (19) becomes, in the IRKC scheme,

$$w_{n1} = w_n + \tilde{\mu}_1 \tau F_E(t_n + c_0\tau, w_{n0}) + \tilde{\mu}_1 \tau F_I(t_n + c_1\tau, w_{n1}) \quad (20)$$

with $\tilde{\mu}_1$ as defined before. Note that the highly stiff part of F is treated implicitly. The other $(s-1)$ subsequent stages of (19) are modified similarly.

With respect to stability of this IMEX extension of (19), it can be remarked that the implicit part is unconditionally stable, whereas the stability condition for the explicit part remains unchanged [13]. Unconditional positivity is not ensured for this scheme.

5.2 Nonlinear and Linear Solvers

The nonlinear systems coming forth from the time discretizations described in the previous section are solved by Newton's method. The disadvantage of local convergence can be overcome by implementing an Armijo type algorithm. For more details we refer to [14] and to [5] for implementation details.

The linear systems within the Newton algorithm are solved by a LU factorization with diagonal scaling. To reduce the amount of work, a reordering of the unknowns and equations has been done. This reordering reduces the bandwidth of the Jacobian considerably, thus reducing the amount of fill in and saving computational costs. For details, we refer to [5,6].

Current research includes the incorporation of iterative linear solvers, which is not straightforward. The linear systems are recognized by huge condition numbers, which influence the convergence behavior. Second, the behavior with respect to positivity is unpredictable.

5.3 Variable Time Stepping

We briefly explain the variable time-stepping algorithm as it is implemented in our code. Consider an attempted step from t_n to $t_{n+1} = t_n + \tau_n$ with time step size τ_n that is performed with a pth-order time integration method. Suppose an estimate D_n of order $\hat{p}$ of the norm of the local truncation error is available. Then if $D_n < Tol$, this step τ_n is accepted, whereas if $D_n > Tol$, the step is rejected and redone with a halved time step size. If $D_n < Tol$, then the new step size is computed as

$$\tau_{\text{new}} = r\tau, \quad r = \left(\frac{Tol}{D_n}\right)^{1/(\hat{p}+1)} \quad (21)$$

By giving bounds on r, it is possible to put bounds on the growth factor r of the new step size. Furthermore, an attempted time step from t_n to t_{n+1} is also rejected when the solution on time t_{n+1} has negative species concentrations. In that case we halve the time step size, $\tau_n \leftarrow \frac{1}{2}\tau_n$, and recompute the solution on time t_{n+1}. Details can be found in [5,9].

6. NUMERICAL RESULTS

In this section, we compare the performance of the different time integration methods of Section 5.1 to solve the species equations (5), with nonlinear and linear solvers as mentioned in Section 5.2.

Since the gas mixture is highly diluted by the carrier gas helium He, we used the steady-state velocity, density, temperature, and pressure fields computed by Kleijn [3] for our transient simulations. Finding the solutions of these fields is a rather trivial task in comparison with solving the time-dependent species equations. Our transient simulations run from initial conditions, where the reactor is completely filled with helium carrier gas, and a mixture of silane diluted in helium starts to enter the reactor, into steady-state. Thereafter, we compare our steady-state solution with the one obtained in [3]. Actually, in the present simulation, thermal diffusion (Soret effect) was neglected. Therefore, the results were compared with results obtained with the code used in [3], recomputed without thermal diffusion. For the sake of clarity, we considered the case with wafer temperature $T_s = 1000$ K and a nonrotating disk, see also [3].

In Table 2, the integration statistics for the schemes discussed in Section 5 can be found for the simulations with and without reacting surface. Inclusion of surface chemistry changes the physics of the system, resulting in different integration statistics. In this case, we observed for all schemes except IRKC longer CPU times, and more sensitive behavior of the Newton method and for positivity. For the IRKC scheme with included surface chemistry, we measured shorter simulation times, but the difference between both is for CPU times in the region of noise.

TABLE 2. Integration statistics of EB, ROS2, BDF-2, and IRKC running into steady-state (performed on a Pentium IV 3.2 GHz). Number of F-evaluations for IRKC are the ones containing reaction terms

	Without Surface Chemistry				Including Surface Chemistry			
Number of	EB	ROS2	BDF-2	IRKC	EB	ROS2	BDF-2	IRKC
F	192	551	510	71,306	491	2114	3697	77,480
F'	74	191	241	450	231	802	1402	10,18
Linesearch	28	0	42	0	68	0	24	0
Newton iters	74	0	241	18,016	231	0	1402	19,500
Rej. time steps	0	22	14	156	5	292	489	370
Acc. time steps	37	169	92	294	94	510	893	648
CPU Time	5500	12,700	23,280	13,800	10,900	$\pm$40,000	$>$ 50,000	12,900

For IRKC, the number of function evaluations and total number of Newton iterations seems to be quite high. However, we have to remark that the Newton process in the IRKC is cheaper than for the other ODE methods [13]. Self-evidently, when the number of nonlinear systems increases, also the number of F evaluations containing the reaction terms increases.

The deposition rate of solid silicon (10) along the symmetry axis in the benchmark problem is $2.49\ \mathrm{nm/s}$ [3]. In all our simulations, we measured a deposition rate of $2.43\ \mathrm{nm/s}$ in steady-state. The transient behavior of this deposition rate is monotone, increasing in time toward this value. Furthermore, Fig. 3 shows mass fraction profiles for some selected species, as a function of the height above the wafer at the symmetry axis. We conclude that the steady-state solutions and deposition rates obtained by our transient code agrees well with the results obtained with the code used in [3].

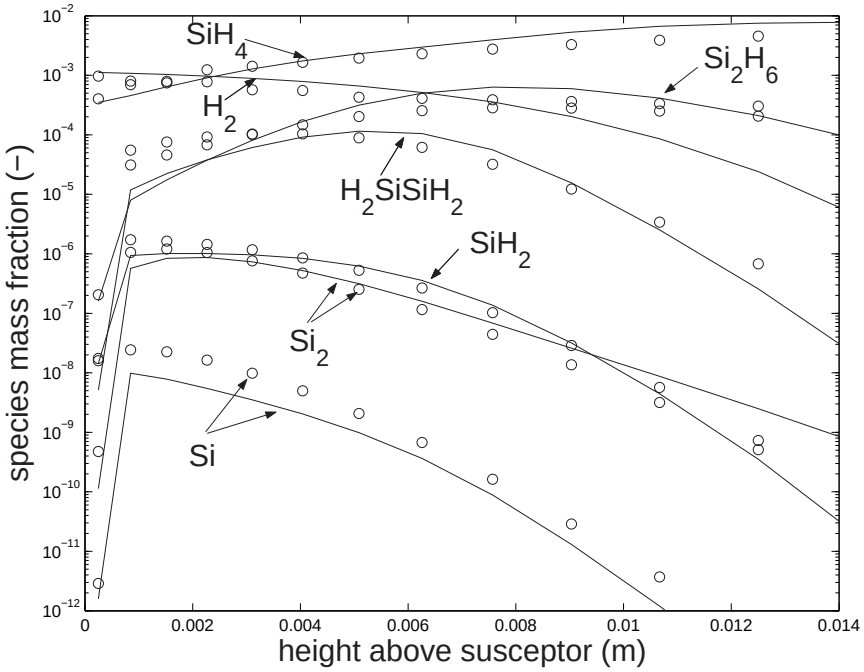

FIGURE 3. Steady-state axial mass fraction profiles for some selected species. A similar figure can be found in [3]. Solid lines: profiles obtained with the code of [3]. Circles: our steady-state mass fraction profiles

7. CONCLUSIONS

We compared a selection of ODE integration methods that are suitable for transient simulations of stiff systems of species equations that appear in CVD and other laminar reacting gas flows. We observe that inclusion of surface chemistry, where actually more "fast" components are added to the system, results in increasing computational costs. This can be explained by the fact that to correctly follow faster processes needs smaller time steps.

Our computational results are actually a comparison of ODE methods, because the nonlinear and linear solvers are not individually optimized for each ODE method. Based on the observations in our experiments, we conclude that EB is the most efficient time integrator. However, for 3D transient simulations the IRKC scheme is still an excellent candidate because the associated nonlinear systems can be solved in a cheaper way.

ACKNOWLEDGMENT

Thanks are addressed to Dr. B. P. Sommeijer from the CWI in Amsterdam for his suggestions to improve the performance of our IRKC code.

REFERENCES

1. Hitchman, M. L., and Jensen, K. F., *Chemical Vapor Deposition—Principles and Applications*, Academic Press, London, 1993.
2. Kee, R. J., Coltrin, M. E., and Glarborg, P., *Chemically Reacting Flow: Theory and Practice*, Wiley, New York, 2003.
3. Kleijn, C. R., Computational modeling of transport phenomena and detailed chemistry in chemical vapor deposition—A benchmark solution, *Thin Solid Films* **365**:294–306, 2000.
4. Kleijn, C. R., Transport Phenomena in Chemical Vapor Deposition Reactors, Ph.D. thesis, Delft University of Technology, Delft, 1991.
5. van Veldhuizen, S., Vuik, C., and Kleijn, C. R., Numerical Methods for CVD Simulation, Technical Report, Delft University of Technology, Report No. 06-07, Delft, 2006.
6. van Veldhuizen, S., Vuik, C., and Kleijn, C. R., Numerical Methods for Reacting Gas Flows, In *Lecture Notes in Computational Science 3992, Proc. of ICCS 2006,* Reading, May 2006. V. N. Alexandrov et al., Eds. Springer, Berlin, 10–17, 2006.
7. Coltrin, M. E., Kee, R. J., and Evans, G. H., A mathematical model of the fluid mechanics and gas-phase chemistry in a rotating disk chemical vapor deposition reactor, *J. Electrochem. Soc.* **136**:819–829, 1989.
8. van Veldhuizen, S., Vuik, C., and Kleijn, C. R., A Note on the Numerical Simulation of Kleijn's Benchmark Problem, Technical Report, Delft University of Technology, Report No. 06-15, Delft, 2006.
9. Hundsdorfer, W., and Verwer, J. G., *Numerical Solution of Time-Dependent Advection-Diffusion-Reaction Equations*, Springer Series in Computational Mathematics, vol. 33, Springer, Berlin, 2003.
10. Bolley, C., and Crouzeix, M., Conservation de la positivité lors de la discrétisation des problèmes d'évolution paraboliques, *RAIRO Anal. Numer.* **12**:237–245, 1973.
11. *TNO CVD-X User Manual*, Version 4.0, TNO Science and Industry, support.glassgroup@tno.nl
12. Verwer, J. G., Spee, E. J., Blom, J. G., and Hundsdorfer, W., A second-order rosenbrock method applied to photochemical dipersion problems, *SIAM J. Sci. Comp.* **20**:1456–1480, 1999
13. Verwer, J. G., Sommeijer, B. P., and Hundsdorfer, W., RKC time-stepping for advection-diffusion-reaction problems, *J. Comp. Phys.* **201**:61–79, 2004.
14. Kelley, C. T., *Solving Nonlinear Equations with Newton's Method*, Fundamentals of Algorithms, SIAM, Philadelphia, 2003.